# Insight into the gas-phase glycerol dehydration on transition metal modified aluminium phosphates and zeolites

***Susana Lopez-Pedrajas*, Rafael Estevez, Fatima Blanco-Bonilla, Diego Luna and Felipa M. Bautista****

*Departamento Química Orgánica, Instituto de Química Fina y Nanoquímica, Universidad de Córdoba, Campus de Excelencia Internacional Agroalimentario CeiA3. Edificio Marie Curie, E-14014 Córdoba, Spain. E-mail:*rafa_20_15@hotmail.com, **fmbautista@uco.es*

## Abstract

**BACKGROUND:** The production of biodiesel has notably increased in years, with glycerol as the main by-product, an important raw material in the production of value-added products. Those obtained by dehydration are especially important.

**RESULTS:** Gas phase dehydration of glycerol has been tested on mesoporous AlPO4 andmodified AlPO4, with a small amount (1 wt%) of a transitionmetal (Co, Cu, Cr, Fe), calcined at 450∘C and 650∘C, and comparedwith some commercial zeolites (HZSM and HY). All the catalysts were active in the reaction, the posphates showing better catalytic behaviour than the zeolites. The main products of the reaction were acrolein and hydroxyacetone.

**CONCLUSIONS:** The positive effect of metal on the catalytic behaviour of AlPO4 in the dehydration has been verified, attaining the maximum yield to acrolein (54%) on AlCoPO650 with 50 mg of catalyst and 280∘C of reaction temperature. Furthermore, the phosphates did not suffer deactivation after 22 h reaction, whereas the zeolites suffered a strong loss of activity (around 0%) due to blockage of themicropores by coke. Moreover,

the yield to acrolein decreased with time, while the yield to hydroxyacetone increased. An E2 mechanism for the acrolein formation and E1 for the hydroxyacetone formation have been proposed.

Keywords: glycerol; acrolein; hydroxyacetone; metal-aluminium phosphates; zeolites; deactivation

## Introduction

In recent years, the production of biodiesel has notably increased. According to theFAO (Food and Agriculture Organization) this tendency is going to continue in the future, but at a slower rate than in the past.[1] Biodiesel production by transesterification of triglycerides generates glycerol (1,2,3-propanetriol) as the main by-product. This fact has led to a drastic surplus of glycerol in the chemical markets.[2,3] The composition of the crude glycerol, obtained directly from biodiesel production, generally oscillates between 50 and 80% glycerol, 3–15% water, 5–15% salt, <1–20% methanol, 1–5%fatty acids and 1–5% non-glycerol organicmaterial, by weight.3 This crude glycerol has little value due to its impurities, thus employing it to produce value-added products would increase its value. Among these products, those obtained from glycerol dehydration, propen-2-al or acrolein (ACR) and hydroxyacetone (HA) or acetol, are especially important. ACR can be used as a raw material to produce DL-methionine and acrylic acid and its derivatives,whereas HA is an intermediate for the production of propanediols and can be used as a flavour in the food industry, as dyes, as additives in cosmetics and so on. Glycerol dehydration reaction has been investigated mainly on heterogeneous catalysts, as has been indicated in recent reviews.[4,5] Typically, the reaction is carried out in the temperature range 250–350∘C using aqueous glycerol as a feedstock, which is advantageous because glycerol is usually obtained mixed with water, as aforementioned. Furthermore, the reaction in gas phase generally occurs with better results than in liquid phase, as we have previously reported.[6,7] The acidity of the catalyst plays an important role not only in its activity and selectivity in glycerol dehydration, but also in its stability or resistance to deactivation. However, there is no agreement in the literature about the nature and strength of the acid sites implied in the formation of the main dehydration products. Thus, Chai et al.[8] based on the study of various solid catalysts with a wide range

of acid-base properties reported that acrolein formation is enhanced by strong acid sites, mainly Bronsted acid sites, whereas the basic solids hardly showed any selectivity to acrolein. Likewise, some recent studies have proposed that the formation of acrolein takes place on Brönsted acid sites[9–12] and that of hydroxyacetone on Lewis acid sites.[9,12] Foo et al.[10] have demonstrated the cooperative role of Brönsted and Lewis acid sites in the glycerol dehydration to hydroxyacetone over niobia catalysts, whereas, Wang et al.[13] indicated this cooperative effect but for the acrolein formation. Kinage et al.[14] on sodium-doped metal (Ce, Al, Ga, Zr) oxides even reported the participation of the basic sites in the formation of HA, proposing a complicated reaction scheme implicating three steps: glycerol dehydrogenation, dehydration of the obtained compound and rehydrogenation of this latter. More agreement seems to exist about the participation of the very strong acid sites, mainly Brönsted sites, in the coke formation,[6–8,12,15] which provokes catalyst deactivation, mainly by pore blocking. The microporous materials being more quickly and widely deactivated than those proving to be meso or macroporous.[8,16,17] On this basis, the aim of the present research is to verify the influence of the acid sites (nature and strength) and textural properties of the catalysts on its activity and stability in the formation of glycerol dehydration products in the gas phase, as we previously demonstrated in liquid phase.[7] Thus, we have studied materials such as a mesoporous aluminium phosphate (AlPO4) and different zeolites (HZSM and HY). Furthermore, we have also studied the influence of a second metal (Co, Cu, Cr, Fe) on the catalytic behaviour of aluminium phosphate. In previous work,[6] we demonstrated the favourable effect of a metal with redox properties, such as vanadium, on the activity in the acrolein formation of AlPO4, whereas Ca did not have this effect. The solids have been characterized by X-ray diffraction (XRD); scanning electron microscopy (SEM); $^{31}P$ and $^{27}Al$ magic angle spinning nuclear magnetic resonance (MAS NMR) and diffuse

reflectance ultraviolet-visible (DR-UV-Vis) spectroscopy. Their acid properties were determined from temperature programmed desorption (TPD) and diffuse reflectance infrared Fourier transform

(DRIFT) of adsorbed pyridine. Furthermore, the test reaction of 2-propanol transformation in the absence of oxygen was also employed in evaluating the acid sites (responsible for dehydration to propene) and the basic/redox sites (responsible for propanone formation) of the solids. Astudy on the formation and nature of coke over time on stream, has also been carried out. In this respect, an off-line analysis of the effluent from the reactor was carried out in order to avoid deposits of unidentified compounds, which were responsible for som obstruction of the reaction system lines, as previously reported.[6]

## Experimental

*Catalyst preparation*

Aluminium phosphate ($AlPO_4$) was prepared by a sol–gel method previously reported.[18–20] It was synthesized from $AlCl_3.6H_2O$ and $H_3PO_4$ (85 wt%) by precipitation with aqueous ammonia unde stirring at 0 C. The precipitate was allowed to stand at room temperature and the pH value at the 'end point' was 6.7. After filtration, the solid was washed with 2-propanol, dried at 120 ºC for 24 h and calcined in air at 450 ºC for 3 h. The binary system of Co, Cu, Cr and Fe[18] were prepared from an aqueous solution with the appropriate amounts of $AlCl_3.6H_2O$, of the corresponding nitrate and of $H_3PO_4$ in order to obtain a molar ratio P/Al+M=1 and equivalent to th theoretical molar ratio Al/M=49, 52, 42 and 50, respectively. Th metal percentage added in those systems was 1 wt%. They wer calcined in air at 450 ºC and 650 ºC for 3 h. These systems will be denoted as AlMPOT, where T indicates the calcination temperature. For comparative purposes, another solid was prepared with Al and Co (Al-CoPOT) changing for order in which the metal salt and $H_3PO_4$ were added. Thus, $AlCl_3.6H_2O$ was dissolved in water, $H_3PO_4$ was then incorporated and finally, $Co(NO_3)_2.6H_2O$, after stirring. From this point the procedure continued as has been previously described. All the solids were screened at <0.149 mm to avoid internal diffusion limitations in the reactions. Three commercial zeolites from Zeolyst[7] were used: two were ZSM-5 in the $NH_4^+$ form with a different $SiO_2/Al_2O_3$ ratio (CBV 5524G and CBV 3024E), and the other was zeolite HY (CBV 600).7 The ZSM zeolites were converted into the H form after activation in a stream of dry air for 6 h at 600 ºC. This same thermal treatment was employed for the HY(5.2) zeolite. These solids will be denoted as H-ZSM-5(50); H-ZSM-5(30) and HY(5.2), where the number in brackets indicates the $SiO_2/Al_2O_3$ ratio.

*Characterization of the catalysts*

X-ray diffraction (XRD) patterns were performed on a diffractometer (Siemens D-5000), equippedwith an automatic control system. A Ni-filtered, graphite monochromator, Cu K$\alpha$ radiation ($\lambda$=1.5406Å) was used, operating at 35 kV and 20 mA. The samples were scanned $2\circ \leq 2\theta \leq 80\circ$ at a speed of $2\circ$ $min^{-1}$. Scanning electron microscopy (SEM) studies were carried out in a Jeol apparatus, model JSM 6300, equipped with an Oxford Instrument detector, model Link ISIS which allows the chemical analysis by energy dispersion of X-rays (EDX) of the studied solid surface. The measurements were repeated at least three times on different zones of the solid surface (experimental error≤7%). Diffuse reflectance spectra in the UV-Vis region (200–800 nm) were collected at room temperature with a Variant Cary 1E UV-Vis spectrophotometer equipped with reflectance attachment using $BaCl_2$ as reference. $^{31}P$ and $^{27}Al$MAS NMR spectra were collected on a Bruker Avance 400WB spectrometer using a 4mmBruker double resonance MAS probe. All experiments were performed nominally at room temperature. $^{27}Al$ and $^{31}P$ MAS NMR were recorded at resonance frequencies, $\upsilon$0, of 104.26 and 161.98 MHz and $Al(H_2O)_6^{3+}$ and $H_3PO_4$ solutions were used as external standard, respectively. The data were processed by Fourier transformation, phase correction and baseline correction using the Dm2005test NMR data processing software. The textural properties (BET surface area, SBET, pore volume, Vp, and average pore diameter, dp) were obtained from $N_2$ adsorption–desorption isotherms, at liquid nitrogen temperature (77 K), using a Micromeritics ASAP 2000 instrument. Before measurements, all samples were degassed to 0.1 Pa. The pore size distribution has been determined using the Barrett, Joyner and Halenda (BJH) method, assuming a cylindrical pore model. The surface area values were calculated by applying the BET equation at relative pressures in the range p/p0 =0.05–0.30, assuming a cross-sectional area of 0.162 $nm^2$ for the nitrogen molecule. Total acidity

was measured by temperature programmed desorption of pyridine (Py-TPD), using an apparatus from PID Eng&Tech equipped with a TCD (thermal conductivity detector). Before starting the adsorption experiments, the catalyst (30 mg) was pre-treated in situ from room temperature to 400 ºC (rate of 20 ºC per min). After the catalyst pre treatment, saturation of the sample with pyridine was carried out at 50 ºC for 30 min, thereafter, physisorbed pyridinewas desorbed at 50 ºC for 60 min. Then, the measurements were performed in the range of 50–450 ºC, with a heating rate of 10 ºC per min to remove the chemisorbed pyridine. The exceptions were the zeolites, in which the maximum temperature in the pretreatment and in the measurements was 500 ºC and 550 ºC, respectively. Diffuse reflectance infrared Fourier transform (DRIFT) spectra of adsorbed Pyridine were recorded on a FTIR instrument (Bomem MB-3000) equipped with an 'environmental chamber' (Spectra Tech) placed in a diffuse reflectance attachment (Spectra Tech, Collector). A resolution of 8 $cm^{-1}$ was used with 256 scans averaged to obtain a spectrum from 4000 to 600 $cm^{-1}$. The reference spectrum of the sample was recorded at 350∘C. Pyridine (99.8% from Aldrich) adsorption was carried out at 120∘C for a certain period of time (typically 1 h) allowing saturation of the catalyst surface. The samples were subsequently degassed in four steps of 1 h each at 50, 150, 200 and 300 ºC, respectively. The 2-propanol conversion was carried out in a continuous-flow fixed bed micro-catalytic reactor (4 mm internal diameter and 90 mm long) at atmospheric pressure. The catalyst (20 mg, <0.149 nm) was pretreated by in situ heating under nitrogen (20 mL min−1) for 30 min at 300 ºC. The 2-propanol (99.5% from Panreac) was fed by means of a microfeeder at 0.6 mL $h^{-1}$ (2.19 μmol s−1) and the flow of nitrogen was 20 mL min−1. The catalytic measurements were performed at 170, 190, 210 and 230 ºC. The final values reported are the average of six values obtained after the stationary state was attained (15 min). The reaction products (propene, propanone and diisopropyl ether), as well as the 2-

propanol unconverted were analysed by gas chromatography (CG) with a flame ionization detector (FID), by using a capillary column (60m× 0.25mm× 0.25 μm) DB WAX (100%, polyethylene glycol). Under these conditions, no diffusional limitations exist. The estimated experimental error was <4%. The catalysts did not suffer deactivation. Raman spectra were acquired with a Renishaw Raman instrument (inVia RamanMicroscope) by excitation with green laser light (532 nm) and a grating of 1800 lines per mm. A total of 50 scans per spectrum were performed in order to improve the signal-to-noise ratio, with an exposure time of 15 s. Coke determinationwas carried out by thermogravimetric analyses (TGA) using a Setaram Setsys 12 thermobalance in the presence of static air with a 20 mg sample. The heating rate was 10∘Cmin−1 (temperature range: 30–1000 ºC).

*Catalytic test*

Glycerol transformation was carried out in a continuous-flow fixed-bed microreactor (0.35 cm internal diameter and 9 cm long) under atmospheric pressure. Reaction products together with unconverted glycerol were collected in two consecutive ice traps and they were analysed without preliminary extraction or separation of water. The analysis was carried out by gas chromatography (GC) equipped with a flame ionization detector (FID) using a 100% poly(ethylene glycol) (25 m× 0.25 mm× 0.25 μm) capillary
column. The catalyst (50 mg, <0.149 mm) was pretreated at the reaction temperature 280∘C, for 2 h in a N2 flow (50 $cm^3$ $min^{-1}$). A 36 wt% glycerol (99.5%, Sigma–Aldrich) aqueous solution was fed at 0.3 mL $h^{-1}$ ($1.27 \times 10^{-3}$ mol $h^{-1}$), which resulted in a contact time of 2.38 g cat min $mmol^{-1}$. In general, each catalytic test was conducted for 22 h. The products were identified through chromatographic patterns and/or GC-MS (Varian CP 3800, Quadrupole MS 1200) equipped with a Supelcowax 10 (100% poly(ethylene glycol), 30 m× 0.25 mm× 0.25 μm) capillary column. A blank test showed

the absence of homogeneous reactions and the inactivity of the reactor in the absence of a catalyst. In order to avoid the polymerization of acrolein,[21] hydroquinone was added (0.2 wt%) to the aqueous solution of glycerol in the feed and also to the cold trap where the reaction products were collected. The hydroquinone also allowed the carbon balance to be estimated. The absence of hydroquinone reactivity has been verified by tests carried out, with or without this compound under reaction conditions. The glycerol conversion ($X_{Gly}$) was calculated from $X_{Gly} = (mol_{Gly,in}\text{-}mol_{Gly,out}) \cdot 100/mol_{Gly,in}$, whereas the selectivity (Si) and the yield (Yi) to product i were expressed as mol% on a C atom basis.

## Results and discussion

*Structural and textural characterization of the solids*

The XRD patterns (not shown) of the phosphates showed only a very broad hump in the range $2\theta$ between 15 and 40 º, a characteristic of amorphous metal phosphates, regardless of the metal added and the calcination temperature. However, the commercial zeolites showed a crystalline character.[7] Both H-ZSM zeolites exhibited a similar XRD pattern which corresponds with a MFI structure, whereas the HY(5.2) exhibited a Faujasite structure. The micrographs obtained by SEM (Fig. 1) confirmed the amorphous character of the solids also showing a very unhomogeneous distribution in morphology and particle sizes, independently of the presence of one or two metals on the solid, as well as the calcination temperature. With regard to the shape of the particles, both elongated and rounded particles were observed. In comparison with the theoretical composition [Al/M=49 (Co), 42 (Cr) and 50 (Fe)], the modified aluminium phosphates showed a superficial enrichment of M according to the results obtained by EDX analysis, Table 1. This fact was emphasized in the solids calcined at 650 ºC, as well as in Al-CoPO in comparison with AlCoPO. $^{31}$P and $^{27}$AlMAS NMR spectra of the solids studied are collected in Fig. 2. For all the phosphates, the $^{31}$P NMR showed a single peak around –25 ppm, typical of amorphous aluminium phosphates, which can be assigned to P atoms in tetrahedral coordination. Hence, the environments of phosphorus nuclei are mainly $P(OAl)_4$.[22,23] On the other hand, the $^{27}$Al NMR of the different phosphates showed a main resonance at approximately +38 ppm, which is typical of tetrahedral aluminium sharing oxygen atoms with four phosphorus tetrahedrals ($Al(OP)_4$). Other small resonances at +14 and –13 ppm are ascribed to Al species partially coordinated with hydroxyl groups in octa- and pentahedral coordination, respectively.[22–24] With the presence of a second

metal in the $AlPO_4$a slight increase of both components was observed, especially in Al-CoPO450 and AlFePO450.

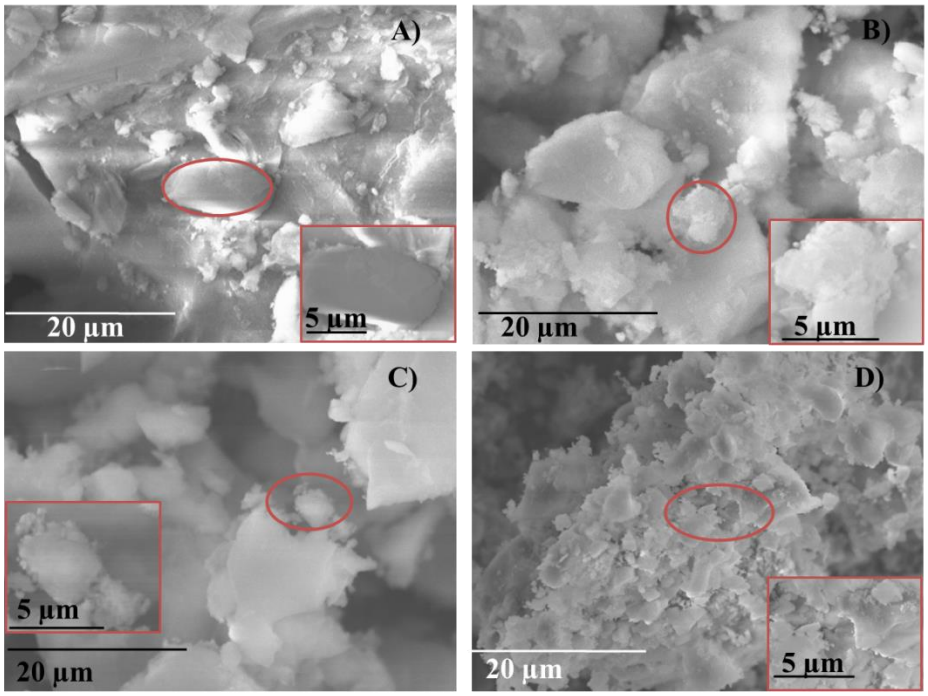


**Figure 1.** SEM micrographs: (A) $AlPO_4$450; (B) Al-CoPO450; (C) AlCrPO450; (D) Al-CoPO650.

**Table 1.** EDX superficial chemical composition and textural properties of the solids studied

| Catalyst | EDX Al/M | EDX P/(M + Al) | $S_{BET}$ ($m^2\ g^{-1}$) | $V_p$ ($mL\ g^{-1}$) | $d_p$ (Å) | Pore size distribution (%) >500 Å | 500-20 Å | <20 Å |
|---|---|---|---|---|---|---|---|---|
| $AlPO_4$450 | - | 1.08 | 199.1 ± 0.8 (137.6 ± 0.4) | 0.82 (0.60) | 165 (175) | 12 (14) | 87 (86) | - (-) |
| AlCoPO450 | 48 | 1.03 | 256.1 ± 0.8 (144.7 ± 0.5) | 0.94 (0.43) | 146 (120) | 13 (22) | 87 (78) | - (-) |
| AlCoPO650 | 43 | 1.04 | 225.5 ± 0.6 | 0.85 | 150 | 14 | 86 | - |
| Al-CoPO450 | 42 | 1.07 | 262.3 ± 0.6 | 0.80 | 122 | 10 | 90 | - |
| Al-CoPO650 | 33 | 1.25 | 243.8 ± 0.7 | 0.77 | 127 | 13 | 87 | - |
| AlCuPO450 | n.d.[a] | - | 213.4 ± 0.7 | 0.82 | 154 | 5 | 95 | - |
| AlCuPO650 | n.d.[a] | - | 201.6 ± 0.7 | 0.82 | 162 | 15 | 85 | - |
| AlCrPO450 | 35 | 1.21 | 262.6 ± 0.7 | 0.82 | 125 | 9 | 91 | - |
| AlCrPO650 | 34 | 1.22 | 247.8 ± 0.7 | 0.79 | 127 | 9 | 91 | - |
| AlFePO450 | 33 | 0.88 | 248 ± 1 (200.1 ± 0.6) | 1.04 (0.79) | 168 (153) | 17 (26) | 82 (76) | - |
| H-ZSM-5(50) | - | - | 425[b] | 0.27 (0.15)[c] | 19.3 | 20 | 29 | 51 |
| H-ZSM-5(30) | - | - | 400[b] (49.2 ± 0.6) | 0.27 (0.12)[c] (0.26) (0) | 22.6 (215) | 23 (79) | 35 (20) | 42 (1) |
| HY(5.2) | - | - | 660[b] (32.4 ± 0.2) | 0.36 (0.20)[c] (0.12) (0) | 23.0 (149) | 21 (60) | 31 (39) | 48 (1) |

In brackets, used catalysts after 22 h.
[a] Not determined.
[b] Data from Zeolyst.
[c] Volume of micropores of the fresh catalysts obtained by the t-plot method.

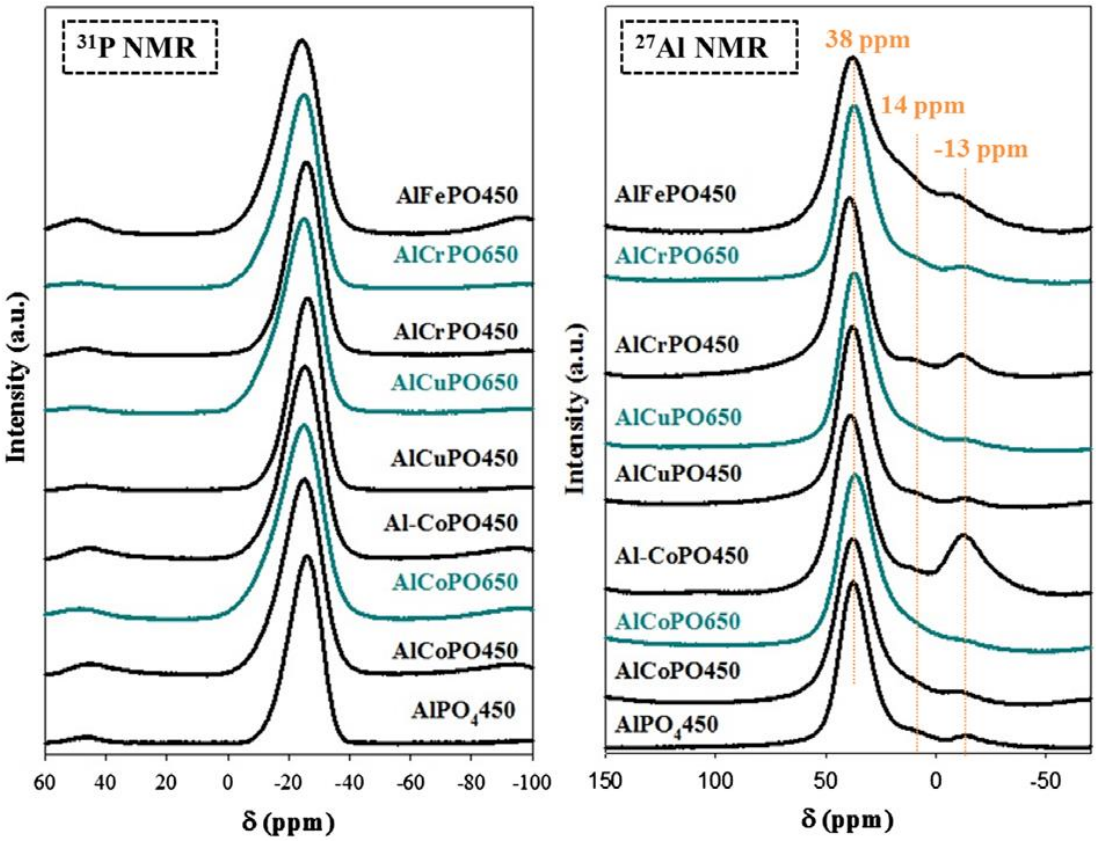


**Figure 2.** $^{31}$P and $^{27}$Al MAS NMR spectra for the phosphates studied.

The UV-Vis spectra obtained for the solids studied and some reference compounds are shown in Fig. 3. Absorption of the$AlPO_4$450 was insignificant in comparison with those of the modified phosphates, therefore we can assume that the absorptions of the modified phosphates are related to the charge transfer between transition metal and oxygen. The oxidation state of each metal was as expected in accordance with the synthesis of modified phosphates. Thus, the aluminium phosphates modified with Co showed similar spectra, with a broad asymmetric band between 530 and 700 nm, with three maxima of absorption that can be assigned to $Co^{2+}$ in a tetrahedral environment.[25] The absorption at 473 nm in the cobalt phosphate spectrum is related with $Co^{2+}$ in an octahedral coordination. The spectra presented another much weaker band at 313 nm, thatwould indicate the presence of some tetrahedral $Co^{3+}$ in the framework of the solid.[25] In the spectra of the solids with Cu, a broad band appeared at 235 nm that is ascribed to the charge transfer transition between $O^{2-}$ and $Cu^{2+}$.[26]

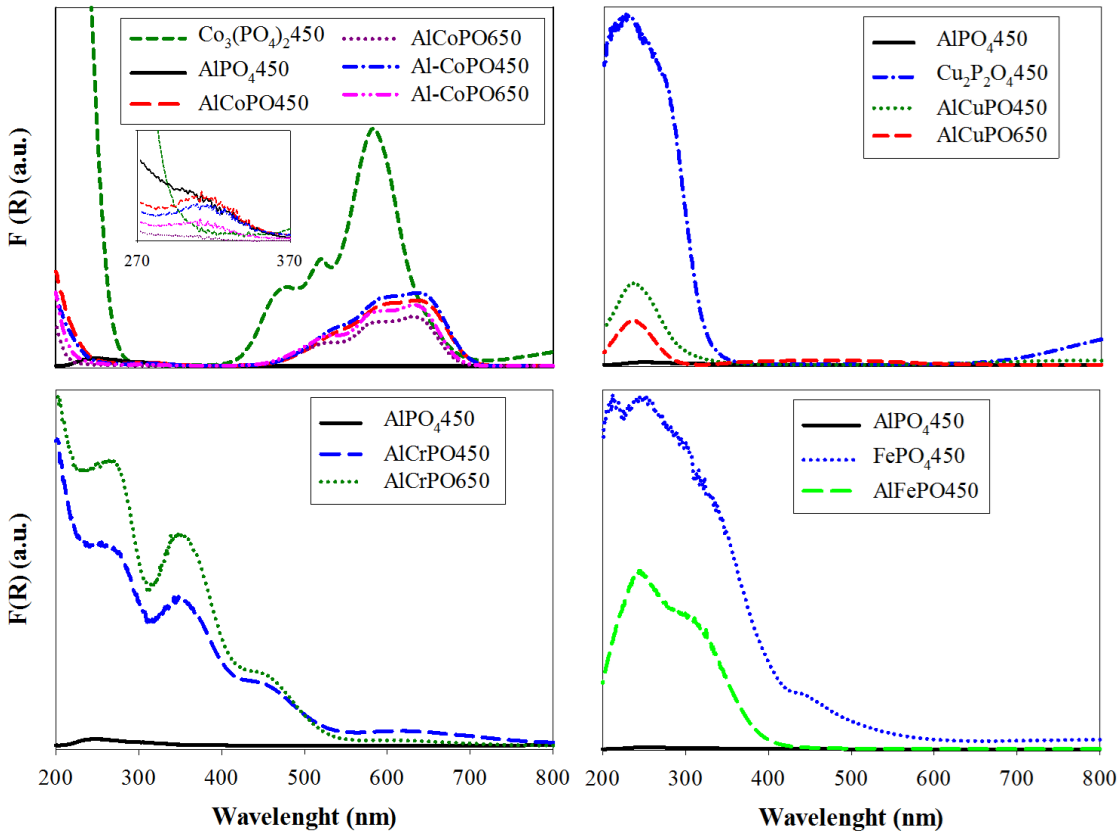


**Figure 3.** UV-Vis spectra.

These samples showed a greenish-blue colour, the pyrophosphate being greener than the binary solids. The spectra of the AlCrPO450 showed four bands. The bands at 266 and 349 nm are normally assigned to Cr6+ of chromate and/or polychromate species,27 the latter could also be ascribed to the third transition of a pseudo-octahedral Cr3+ species.28. The bands at 449 and 618 nm are assigned to d–d transitions of the Cr3+ in distorted octahedral coordination.27 Both samples were yellowish green. The spectrum of the AlFePO4450 as with that corresponding with an iron phosphate, exhibited a broad band with two maxima at 240 and 310 nm, indicating Fe3+ in tetrahedral and octahedral coordination, respectively.18 According to the textural analysis, the nitrogen isotherms obtained for all the metal phosphates studied were type IV of the Brunauer, Deming, Deming and Teller (BDDT) classification, exhibiting type H1 hysteresis loops, which corresponded with mesoporous solids. Table 1 compiles the values of SBET, the pore

volume, the average pore size, as well as the percentage ofmacropores (>500 Å), mesopores (20–500 Å) and micropores (<20 Å) for all the phosphates. As can be seen, the presence of a second metal gave rise to an increase in the SBET between 25 and 32%, except for the AlCuPO450 whose increase was less (7%). On the contrary, the dp value decreased, except for the AlFePO450 which remained almost constant. In addition, the increase of the calcination temperature produced a decrease in the SBET (between 6 and 12%) and a little increase in the dP. It is worth noting that none of the phosphates presented micropores, and the percentages of macropores and mesopores in AlPO4 were not changed significantly by the presence of a second metal. Similar SBET values were obtained for the solids with Co, independently of the synthesis procedure. However, small variations in the VP and dP were observed, being lower in the Al-CoPO system. With regard to the zeolites, they exhibited higher SBET and lower dp and Vp values than metal phosphates, showing around 50% micropores, 20% macropores and 30% mesopores, Table 1.

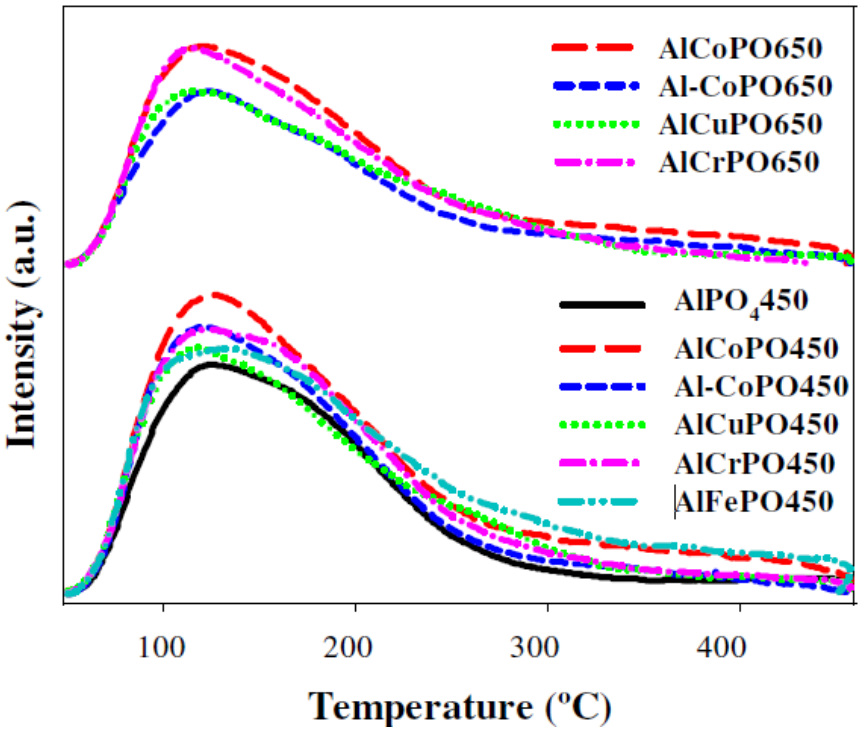


**Figure 4.** Py-TPD profiles observed for the phosphates studied.

*Acid and basic properties*

As far as the acid characterization is concerned, the Py-TPD profiles of the phosphates, Fig. 4, showed a broad band centered between 100 ºC and 200 ºC. As previously reported,[7] the zeolite profiles also showed one maximum peak at around 120 ºC and another of less intensity, around 500∘C. With the exception of Al-CoPO450, AlCrPO650 and HY(5.2) profiles, the others never reached the baseline. The values of total acidity and the percentage of acid sites as a function of their strength are collected in Table 2. The total acidity of the phosphates, as happened with the SBET, increased with the presence of a second metal in the solids with a remarkable rise in the AlFePO450 (39%). Likewise, the increase of calcination temperature promoted a decrease of total acidity. In addition, Al-CoPO exhibited lower total acidity than AlCoPO, which could be due to the highest percentage of cobalt on the surface of Al-CoPO.On the other hand, the density of acid sites of all the phosphates oscillated between 0.5 μmolm$^{-2}$ (Al-CoPO650) and 0.8 μmolm$^{-2}$ (AlFePO450 and AlCuPO450), weak acid sites predominating (≥60%) in all the phosphates. It was remarkable that the AlFePO450 and the AlCoPO systems presented the highest percentage and density of strong acid sites. As far as the zeolites are concerned,[7] both H-ZSM-5 adsorbed approximately the same amount of pyridine, independently of the SiO2/Al2O3 ratio, whereas the HY(5.2) adsorbed the highest quantity of pyridine. Furthermore, the zeolites exhibited a total acidity higher than the majority of the binary phosphates, but a lower density of acid sites. Moreover, all the zeolites showed mainly weak acid sites, as occurred with the phosphates, although the percentage of strong acid sites was superior to that of the phosphates. The HY(5.2) zeolite exhibited the highest percentage and quantity (62 μmol g$^{-1}$) of this type of site. The DRIFT spectroscopy allows distinguishing the nature of acid sites, because adsorbed pyridine shows different bands between 1400 and 1700 cm$^{-1}$ depending on the type of

acid sites. The pyridine adsorption bands around 1440–1460 $cm^{-1}$ correspond to pyridine adsorbed on Lewis sites (L) and bands around 1540–1560 $cm^{-1}$ are associated with Brönsted sites (B).[7,20,29] In general, all the solids exhibited similar spectra to that shown for AlCoPO650 (Fig. 5(A)), indicating that all the solids analysed showed bands associated with both, B and L. In order to estimate which type of acid sites were more abundant and their strength, the B/(L+B) ratio has been calculated at two temperatures, 150º C and 300 ºC desorbed pyridine. The results shown in Table 2 indicate that all the phosphates possess more Lewis acid sites than Brönsted acid sites. Furthermore, the presence of a second metal in the solids, as well as the thermal treatment at a higher temperature produced an increase in the percentage of Lewis acid sites. Regarding the strength of the sites, desorption of pyridine at 300∘C indicated that Lewis acid sites were stronger than Brönsted acid sites. In the case of the zeolites, the opposite occurred; in general, the zeolites[7] exhibited a higher percentage of Brönsted acid sites than the phosphates, Lewis acid sites increased as the Al2O3 increased. In fact the H-ZSM-5(50) exhibited the highest percentage of Bronsted acid sites. Figure 5(B) shows the OH stretching vibration region (3000–4000 $cm^{-1}$) for the AlCoPO650. The band at 3670–3680 cm−1 is assigned to isolated germinal O–H attached to the phosphorus atom or to single P–OH groups, which exhibit nearly the same OH stretching frequencies but different combination frequencies, and the broad band with maximum at 3780–3790 $cm^{-1}$ is the characteristic band of surface Al-OH with Al atoms in tetrahedral coordination.[20,29] The P–OH groups represent the most stable Brönsted acid sites on AlPO4 surfaces, whereas Al–OH would enhance the acidity of the P–OH groups through H-bonding.[20,29] All the solids presented the two bands, which gradually decreased with increase of the degassing temperature. In the zeolites spectra,[7] bands at 3735 $cm^{-1}$ and 3600 $cm^{-1}$ could be assigned to the vibration of terminal silanol groups (Si-OH) located at the external

surface and to the O–H vibration of bridging Si(OH)Al groups located at the internal zeolites surface, respectively. The intensity of the second band diminished more slowly than the first one, indicating higher strength of the bridging OH in comparison with the terminal silanol groups. The transformation of 2-propanol takes place preferably by two reactions: dehydration to propene ($C_3H_6$), mainly on acid sites, and dehydrogenation to propanone ($C_3H_6O$), mainly on basic/redox sites.[22] Furthermore, under certain experimental conditions, such as low temperatures and high partial pressure of 2-propanol, the formation of diisopropyl ether (C6H14O), would be favoured also on acid sites. As can be seen in Table 2, all the catalysts produced propene as the major product (selectivity values >66%) and diisopropyl ether at lower percentage (selectivity values below 16%). Consequently, in all the solids studied the acid sites dominated. Propanone was obtained on all catalysts with the exception of AlPO4450. This result corroborates that previously reported,[22] in the sense that the formation of propanone requires basic sites with redox ability. Unfortunately, the low percentage of transition metal in the $AlPO_4$ did not allow for detection of $H_2$ in the TPR (temperature programmed reduction) experiments. Evaluation of the surface acidity and of the basic/redox sites of the solids was carried out based on the selectivity values to propene and propanone, respectively, obtained at isoconversion. This has been made, given that the values of selectivity to propene increased and selectivity to propanone decreased, as the reaction temperature (or the 2-propanol conversion) increased. The values of selectivity (Si) obtained at isoconversion (≈1 mol%), together with the values of temperature necessary to get such a conversion value, are collected in Table 2. As can be seen, the modified $AlPO_4$ were slightly more active than the aluminium phosphate itself, although the capacity to produce propene, and consequently the acidity, hardly changed, in clear agreement with the results obtained from Py-TPD. The formation of propanone was slightly favoured on the

modified phosphates calcined at 450 ºC. As can also be seen in Table 2, the zeolites exhibited much higher activity than the aluminium phosphates. In fact, only the H-ZSM-5(50) zeolite with the highest SiO2/Al2O3 ratio showed a similar value of conversion (1 mol%) at 170 ºC, also showing a value of selectivity to propanone (17%) similar to those exhibited by the modified aluminium phosphates calcined at 450∘C. The presence of some basic sites in this zeolite has previously been reported.[7]

**Table 2.** Acidity measurements from Py-TPD; B/L + B ratio for each catalyst after pyridine degassing for 1 h at 150°C and 300°C; and temperature and selectivity at isoconversion (≈1 mol%) for 2-propanol decomposition (w = 0.02 g; $F_{C3H8O}$ = 0.6 mL $h^{-1}$)

| | Acidity | | Strength of acid sites (%) | | | Acid sites nature | | 2-propanol conversion | | | |
|---|---|---|---|---|---|---|---|---|---|---|---|
| Catalyst | (μmol $g^{-1}$) | (μmol $m^{-2}$) | Weak (80–200°C) | Medium (200–300°C) | Strong (>300°C) | B/L + B (150°C) | B/L + B (300°C) | $T_{ISO}$ (°C) | $S_{C3H6}$ | $S_{C3H6O}$ | $S_{C6H14O}$ |
| | | | | | | | | | (mol%) | | |
| $AlPO_4$450 | 144 (77)[a] | 0.7 (0.6) | 72 (79) | 20 (15) | 8 (6) | 0.47 | 0.38 | 210 | 85 | - | 15 |
| AlCoPO450 | 186 (133) | 0.7 (0.9) | 66 (54) | 21 (19) | 13 (27) | 0.37 | 0.24 | 170 | 83 | 17 | - |
| AlCoPO650 | 169 | 0.7 | 66 | 21 | 13 | 0.19 | 0.22 | 170 | 88 | 12 | - |
| Al-CoPO450 | 166 | 0.6 | 73 | 20 | 7 | 0.24 | 0.29 | 190 | 75 | 16 | 9 |
| Al-CoPO650 | 127 | 0.5 | 68 | 21 | 11 | 0.22 | 0.15 | 190 | 86 | 4 | 10 |
| AlCuPO450 | 162 | 0.8 | 69 | 23 | 8 | 0.24 | 0.20 | 170 | 87 | 13 | - |
| AlCuPO650 | 133 | 0.7 | 67 | 25 | 8 | 0.19 | 0.13 | 190 | 86 | 11 | 3 |
| AlCrPO450 | 179 | 0.7 | 70 | 22 | 8 | 0.16 | 0.15 | 170 | 82 | 18 | - |
| AlCrPO650 | 151 | 0.6 | 72 | 22 | 6 | 0.15 | 0.15 | 190 | 89 | 5 | 6 |
| AlFePO450 | 200 (115) | 0.8 (0.6) | 60 (50) | 25 (27) | 15 (23) | 0.46 | 0.38 | n.d.[b] | - | - | - |
| H-ZSM-5(50) | 202 | 0.5 | 80 | 3 | 17 | 0.82 | 0.74 | 170 (1)[c] | 83 | 17 | - |
| H-ZSM-5(30) | 187 | 0.5 | 81 | 6 | 13 | 0.47 | 0.61 | 170 (6)[c] | 94 | 2 | 4 |
| HY(5.2) | 281 (32) | 0.4 (1.0) | 67 (92) | 11 (4) | 22 (4) | 0.40 | 0.53 | 170 (32)[c] | 98 | 1 | 1 |

[a] In brackets, used catalysts after 22 h.
[b] Not determined.
[c] Conversión values (mol %) at 170°C (zeolites cannot be compared at isoconversion).

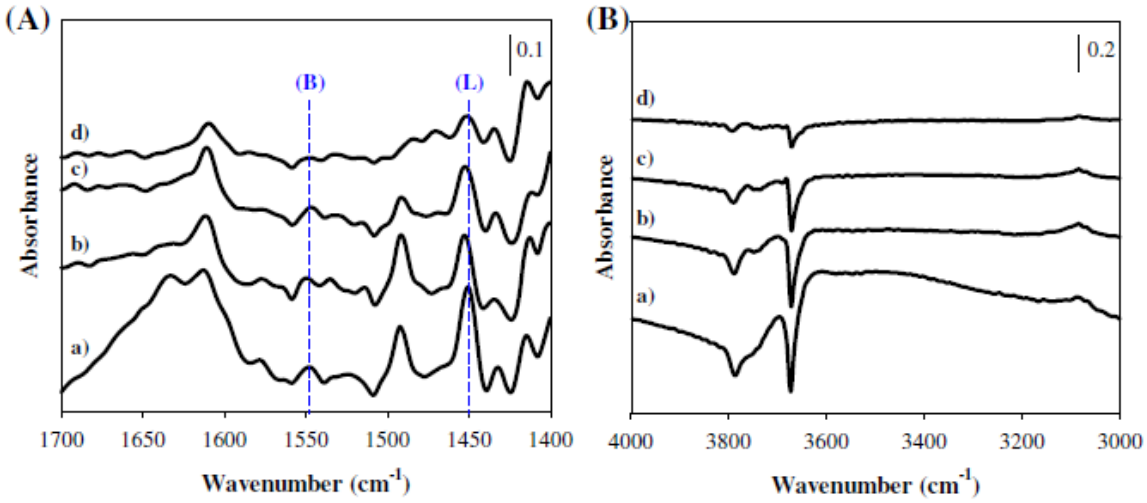


**Figure 5.** DRIFT spectra of adsorbed pyridine after degassing at four different temperatures (a) 50 ºC, (b) 150 ºC, (c) 200 ºC and (d) 300 ºC for 60 min for AlCoPO650 in the region (A)1400 - 1700 $cm^{-1}$ and (B) 4000-3000 $cm^{-1}$.

*Glycerol transformation*

The main products obtained under the experimental conditions studied were ACR and HA. Other by-products were glycerol formal (GF), glycidol (GD) and ethyl glycolate (EG). The possible routes of formation of these products has been discussed elsewhere.6 In addition to these, some unidentified products ('Unknown') were detected, while phenol (P) was also obtained on some catalysts. $CO_2$ was never detected.

*Catalytic activity as a function of time on stream*

The glycerol conversion value increased considerably with the incorporation of a second metal to the $AlPO_4$, regardless of the method of synthesis and thermal treatment used, Table 3. Thus, the conversion values attained at 3 h of operation on modified phosphate calcined at 450 ºC, were double that of AlPO4 (41%), those calcined at 650 ºC exhibiting higher values (around 100%). This increase in the activity of modified aluminium phosphates in relation to the aluminium phosphate cannot be explained based only on their acidity values, which hardly changed, as previously discussed, Table 2. We have to assume the participation of redox sites in the glycerol transformation, responsible for the propanone formation from 2-propanol, associated with the metal introduced in $AlPO_4$, in clear accordance with the results previously reported.[6] Furthermore, the slight metal superficial enrichment existing on the phosphates calcined at 650 ºC, in comparison with those calcined at 450 ºC, would contribute to enhancing the activity. However, the nature of the metal did not seem to play a decisive role in the activity of glycerol, contrary to what was indicated by Suprun[30,31] and Liu.[28] The low percentage of metal employed in the present research, in comparison with that employed by these authors, could explain this fact.

**Table 3.** Values of conversion and yield to reaction products at different times on stream, and amount of coke formed ($mg_C/g_{cat}$) after 22 h of operation. Experimental conditions: 36 wt% glycerol; $F_{Gly} = 0.3$ mL $h^{-1}$; $F_{N2} = 50$ mL $min^{-1}$; w = 0.05 g

| | $X_{Gly}$ (mol%) | | | $Y_{ACR}$ (mol%) | | | $Y_{HA}$ (mol%) | | | Yp (mol%) | | | $Y_{Unknown}$ (mol%) | | | |
|---|---|---|---|---|---|---|---|---|---|---|---|---|---|---|---|---|
| Catalyst | 3 h | 6 h | 22 h | 3 h | 6 h | 22 h | 3 h | 6 h | 22 h | 3 h | 6 h | 22 h | 3 h | 6 h | 22 h | $mg_C/g_{cat}$ |
| $AlPO_4$450 | 41 | 69 | 76 | 20 | 16 | 8 | 9 | 25 | 37 | 1 | 2 | 2 | 6 | 8 | 9 | 242 |
| AlCoPO450 | 86 | 94 | 95 | 44 | 31 | 22 | 25 | 46 | 60 | 7 | 6 | 2 | 4 | 5 | 6 | 235 |
| AlCoPO650 | 100 | 100 | 96 | 54 | 42 | 30 | 29 | 44 | 55 | 13 | 8 | 4 | 4 | 4 | 4 | 66 |
| Al-CoPO450 | 87 | 86 | 94 | 47 | 30 | 22 | 22 | 37 | 61 | 5 | 4 | 2 | 5 | 7 | 5 | 95 |
| Al-CoPO650 | 92 | 90 | 91 | 50 | 26 | 16 | 26 | 45 | 61 | 9 | 6 | 3 | 5 | 10 | 7 | 177 |
| AlCuPO450 | 77 | 89 | 94 | 46 | 33 | 20 | 16 | 42 | 55 | 6 | 6 | 2 | 4 | 4 | 12 | 211 |
| AlCuPO650 | 98 | 98 | 85 | 49 | 33 | 22 | 33 | 49 | 51 | 7 | 4 | 2 | 4 | 6 | 4 | 69 |
| AlCrPO450 | 83 | 92 | 94 | 40 | 36 | 22 | 22 | 40 | 51 | 7 | 4 | 2 | 6 | 5 | 7 | 216 |
| AlCrPO650 | 100 | 100 | 98 | 53 | 38 | 28 | 28 | 42 | 58 | 13 | 7 | 4 | 5 | 10 | 5 | 61 |
| AlFePO450 | 99 | 99 | 93 | 52 | 37 | 14 | 29 | 46 | 65 | 5 | 5 | 2 | 9 | 9 | 9 | 144 |
| H-ZSM-5(50) | 43 | 15 | 13 | 16 | 5 | 3 | 16 | 6 | 5 | 0 | 0 | 0 | 2 | 1 | 2 | 75 |
| H-ZSM-5(30) | 84 | 39 | 17 | 44 | 14 | 3 | 22 | 14 | 8 | 0 | 0 | 0 | 4 | 3 | 2 | 67 |
| HY(5.2) | 48 | 24 | 17 | 18 | 7 | 4 | 23 | 14 | 10 | 0 | 0 | 0 | 2 | 1 | 1 | 142 |

Furthermore, none of the phosphates suffered deactivation after 22 h of operation, Table 3. At this time on stream, the conversion value of $AlPO_4$ was 76%, whereas those of all the modified phosphates were more than 90% (91–98%), with the exception of AlCuPO650 which exhibited a value of 85%. These changes in the conversion values with respect to those obtained at 3 h, were due to the differences in evolution of the conversion values with time on stream, as can be seen in Table 3. Thus, the conversion values on $AlPO_4$ appreciably increased from 3 h (41%) to 6 h (69%), remaining practically constant after 22 h (76%). This same tendency, although less pronounced, was observed for modified phosphates calcined at 450 ºC, whereas the values obtained on those calcined at 650 ºC hardly underwent any changes. These results could be based on the coke formation. In fact, all the catalysts changed from their natural color to black after reaction. Furthermore, the coke formation should take place preferably at the initial stage of the reaction, as proved by the identical TGA profiles obtained for samples of phosphates after 3 h, 6 h and 22 h of reaction (Fig. 6). Therefore, the real conversion values at 3 h should be greater than those shown in Table 3 and, consequently similar to those obtained at 6 h, since the glycerol or reaction products transformed into coke were not taken into consideration. In fact, a higher formation of coke generally implies a lower conversion value at 3 h of reaction, the $AlPO_4$ exhibiting the highest amount of coke (242

mgC/gcat) and the modified phosphate calcined at 650 ºC the lowest (61 mgC/gcat ), as shown in Table 3. As can also be seen in Table 3, in contrast to the phosphates, the zeolites underwent a strong loss of activity with time on stream. Thus, after 6 h of operation the conversion values obtained for the zeolites decreased by half in relation to those at 3 h, showing a value around 15% at 22 h. These results were similar to those reported in the literature; both Chai[8] and Kim[32] used ZSM-5 at 315∘C, losing around 70% and 60% of glycerol conversion, respectively, after 10 h of reaction.

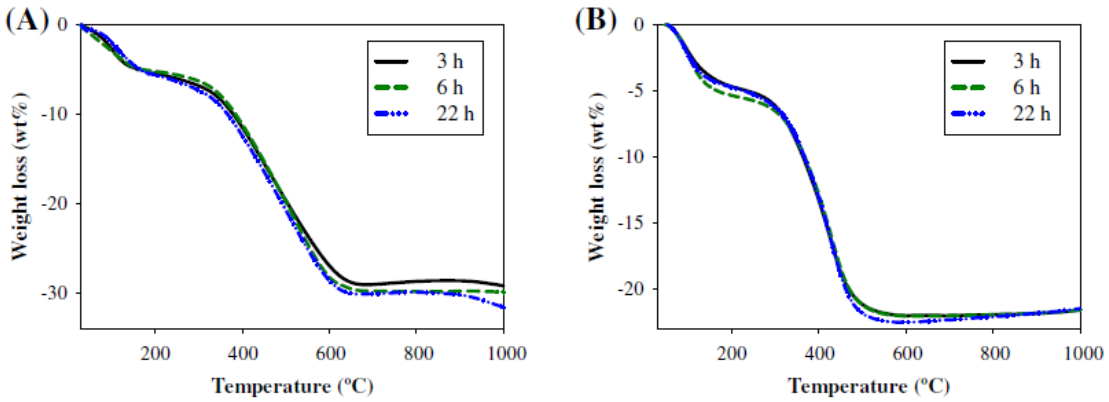


**Figure 6.** TGA analysis of the used (A) AlPO4450 and (B) AlFePO450 at different times on stream.

Furthermore, similarly to that obtained previously in liquid phase[7] the zeolites were less active than the AlPO4 and therefore than the modified $AlPO_4$, at 22 h of operation. However, at 3 h similar activity to $AlPO_4$ (around 45%) was exhibited, with the exception of H-ZSM-5(30), which showed a higher activity, in a likewise manner to the modified $AlPO_4$ calcined at 450 ºC.

The deactivation of the zeolites cannot be explained solely on the basis of the quantity of coke formed, similar to that obtained in the phosphates, but by the different role played by the coke on both types of solid. Thus, the drastic change of the textural properties of the used zeolites, Table 1, with a huge decrease in surface area and pore volume values, suggest that in the zeolites the coke acts by blocking the pores, mainly micropores,

leading to the subsequent loss of acid sites, as shown in Table 2 and Fig. S1 in the Supplementary information. In contrast, the slight decrease in surface area, as well as in pore volume and size suffered by the used phosphates, suggests the formation of coke deposits inside the pores, acting as a poison. In this sense, Dalil et al.[33] have also reported that coke covered the internal walls of the pores rather than plugging the entrances. Although the number of acid sites decreased in a parallel manner with the loss of surface, the density of the acid sites remained within the range exhibited by the fresh phosphates. On the other hand, as a tendency the catalysts with a higher percentage of strong Brönsted acid sites produced a higher amount of coke, which would confirm once again, the participation of this type of acid site in the formation of coke, as indicated in the Introduction. Furthermore, the present results corroborate those previously postulated in liquid phase,[7] in the sense that not only the strong acid sites have influence in the deactivation of the catalysts, promoting coke formation, but also the textural properties. In this context, the low conversion value shown by the HY(5.2) zeolite at 3 h operation, despite being the most active in the 2-propanol transformation, not only among the studied zeolites but also the phosphates, could be explained by a more extensive blockage of its pores by coke, possessing the highest micropore volume.

*Catalyst selectivity as a function of time on stream*

Another general result obtained in the catalytic performance of the phosphates as a function of time on stream, in addition to its high resistance to deactivation, was the change in the production of both main products, acrolein and hydroxyacetone. In effect, the yield to acrolein decreased and similarly, the yield to hydroxyacetone increased as the time of operation advanced, Table 3. Suprun et al.[17,31] reported similar profiles of selectivity to both products over microporous silicoaluminophosphates, $Al_2O_3$ or $TiO_2$ modified with $H_3PO_4$ by impregnation and $PO_4/Al_2O_3$ modified with different transition

metal oxides. The values of yield to acrolein at 3 h oscillated between 44% and 54%, and those to hydroxyacetone between 51% and 65% at 22 h on the modified aluminium phosphates, whereas the values on $AlPO_4$ were 20% and 37%, respectively. These results bring to light once more the positive effect of the modification of AlPO4 with metals, as well as the little influence the type of metal has on the formation of either of the products. However, the systems calcined at 650 ºC and modified with Co and Cr are slightly more active in acrolein formation, while those modified with Cu are more active in that of hydroxyacetone. In this sense, catalysts based on Cu have been reported to be especially active in the formation of hydroxyacetone.[28,31,34,35]

As can be seen in Table 3, the modified aluminium phosphates calcined at 650 ºC also promoted the formation of phenol, attaining yield values of 9 and 13%, which decreased appreciably with time on stream (final values of 3–4%). In contrast, the yield to 'Unknown' products increased with time on stream, $AlPO_4$ and modified $AlPO_4$ calcined at 450∘C being the most active (yield values between 9 and 12% at 22 h of operation). In this same way, the formation of glycidol and ethylglycolate also increased, attaining the highest values, 10% and 5%, respectively, at 22 h on AlPO4. With regard to glycerol formal, its formation did not seem to be affected by the presence of another metal, nor by the time on stream. In either case, the maximum yield obtained did not exceed 8%.

Such a notable change of the main reaction products, acrolein and hydroxyacetone, could be due to an interconversion of Lewis to Brönsted sites, as has previously been reported.[8–10,20,36]

In effect, the water presence in the feed at the reaction temperature, gives rise to a change in the equilibrium between Lewis and Brönsted sites, favouring the formation of Brönsted sites.[20] Thus, the Brönsted acid sites become predominant on the catalyst surface with time on stream, which could favour hydroxyacetone formation over acrolein. In fact, as

shown in Fig. 7 the increase in the ratio HA/ACR with time of reaction was notably higher for $AlPO_4$ and AlFePO450, which initially exhibited a balanced percentage of Lewis and Brönsted acid sites, than for the rest of the phosphates in which the Lewis acid sites predominated.

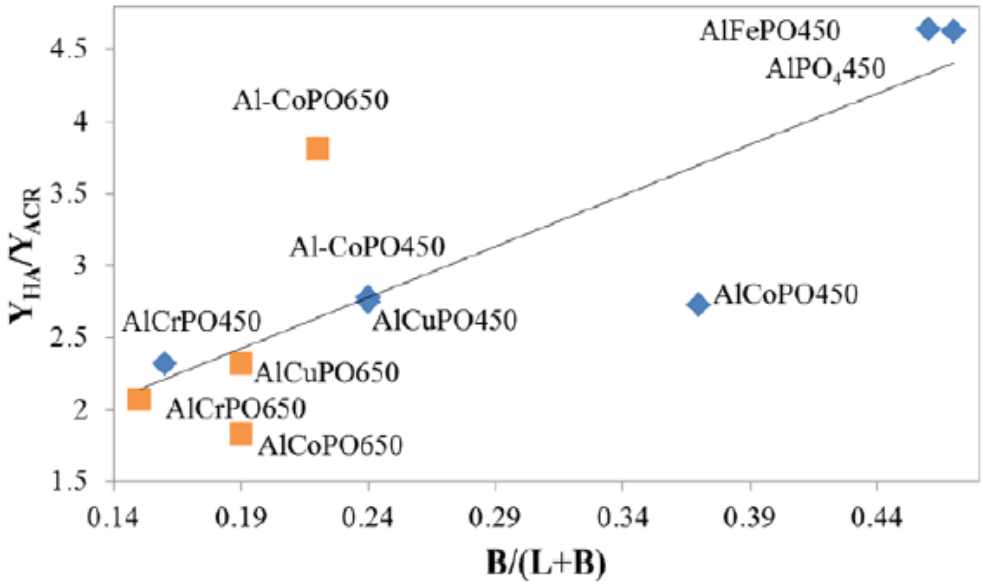


**Figure 7.** Influence of the nature of acid sites (B/B+L after pyridine degassing at 150 ºC, Table 2) on the formation of hydroxyacetone and acrolein (YHA/YACR ratio at 22 h of time on stream, Table 3).

Therefore, the formation of hydroxyacetone preferably through an E1 mechanism, Fig. 8, would be doubly favoured in relation to acrolein due to the existence of two primary hydroxyl groups in the glycerol molecule. At 3 h of time on stream, the Lewis sites were predominant and the glycerol dehydration might take place mainly through an E2 mechanism, involving a pair of Lewis acid and base sites. In this mechanism, the adsorption of a glycerol molecule on a basic site through the hydrogen atoms bonded to primary carbons is twice as likely, Fig. 9, and consequently the formation of 3-hydroxypropanaldehyde, the precursor of acrolein, would be favoured. The transformation of 3-hydroxypropanaldehyde to the more stable aldehyde (acrolein), would easily occur with the participation of either a Brönsted or Lewis acid site. The

participation of the acid (or base) sites caused by the presence of the metal transition, in addition to those related to aluminium, would explain the greater activity exhibited by the modified phosphates in respect to $AlPO_4$.

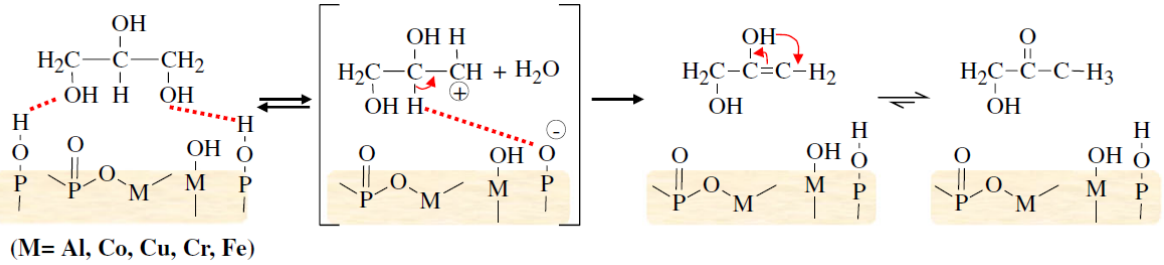


**Figure 8.** Proposed mechanism of hydroxyacetone formation on Bronsted acid sites.

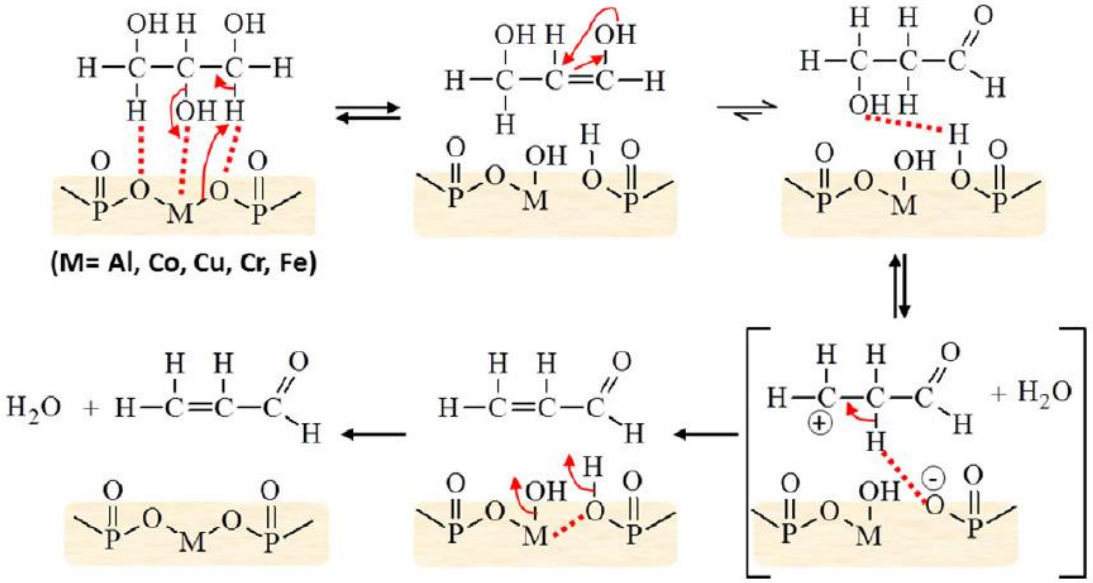


**Figure 9.** Proposed mechanism of acrolein formation on a pair of Lewis acid and base sites.

*Nature of coke*

As Fig. 10 shows, the weight loss (Table 3) was accompanied in some solids by two exothermic peaks around 370 ºC and 510 ºC, in the differential thermal analysis (DTA) curves. These peaks are due to the combustion of coke on the used catalysts, as has been

reported by other authors in the dehydration of glycerol.[17,36-38] Furthermore, an endothermic peak also appeared around 115 ºC, corresponding with the adsorbed water. The first exothermic peak could be assigned to the combustion of a highly hydrogenated carbonaceous species that are easily oxidized, such as aliphatic compounds, while the second peak would be related to the combustion of unsaturated or aromatic compounds, which are more deficient in hydrogen and therefore difficult to burn, as has been previously published.9,36,38 The weight loss of the first peak was considerably less than that corresponding to unsaturated or aromatic species. It was remarkable that both peaks appeared in the solids calcined at 450 ºC, with the exception of the Al-CoPO450, while in the profiles corresponding to the phosphates calcined at 650 ºC, as well as those of the zeolites, only the peak at the highest temperature appeared.

The existence of saturated and aromatic compounds in the coke has been confirmed by Raman and IR spectroscopy, as shown in Fig. 11 for the used $AlPO_4$450. No noticeable XRD peaks representing crystalline carbon were observed for the used catalysts, suggesting that the carbon deposits existed as amorphous carbon species on the catalyst surface; Raman spectra (Fig. 11(A)) showed the band for single-crystal graphite (at 1580 cm−1) and the band for amorphous graphite (1350 $cm^{-1}$).[12] The band around 800 $cm^{-1}$ was related to the deformation vibration of C‑Hbond in aromatic compounds. This information is complemented by that obtained by IR spectra, Fig. 11(B), that were recorded after sample dilution to 15 wt% in KBr and equilibrated for at least 1 h at 280 ºC in a $N_2$ flow of 50 $cm^3$ $min^{-1}$. Thus, the band that appeared at 1700 $cm^{-1}$ is assigned to C=O stretch, whereas those between 1400 and 1600 $cm^{-1}$ to aromatic C=C stretch. In the range 3000-2840 $cm^{-1}$ the bands appeared due to the vibration of the C-H bond of aliphatic compounds, and between 3080 and 3030 $cm^{-1}$ those due to C-H in aromatic

compounds. The band in the region of the vibration of OH (3500-3800 cm−1) assigned to isolated P-OH groups present in the spectra of the fresh solids, is transformed to a broad band in those of the spent catalysts, indicating H-bonded hydroxyls groups.

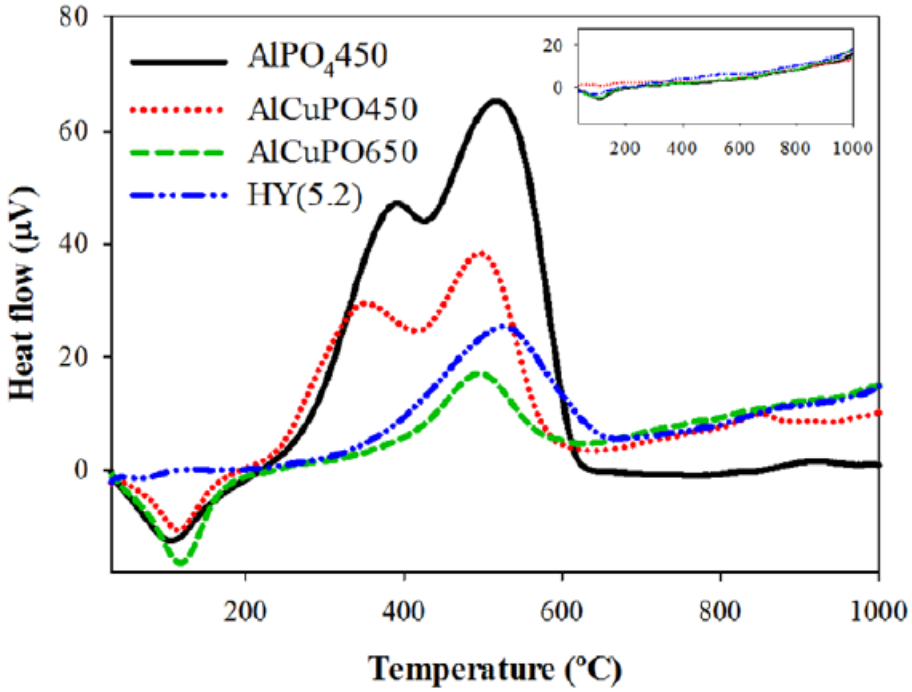


**Figure 10.** DTA profiles obtained for used catalysts. Those of the fresh catalysts appear in the top right-hand corner.

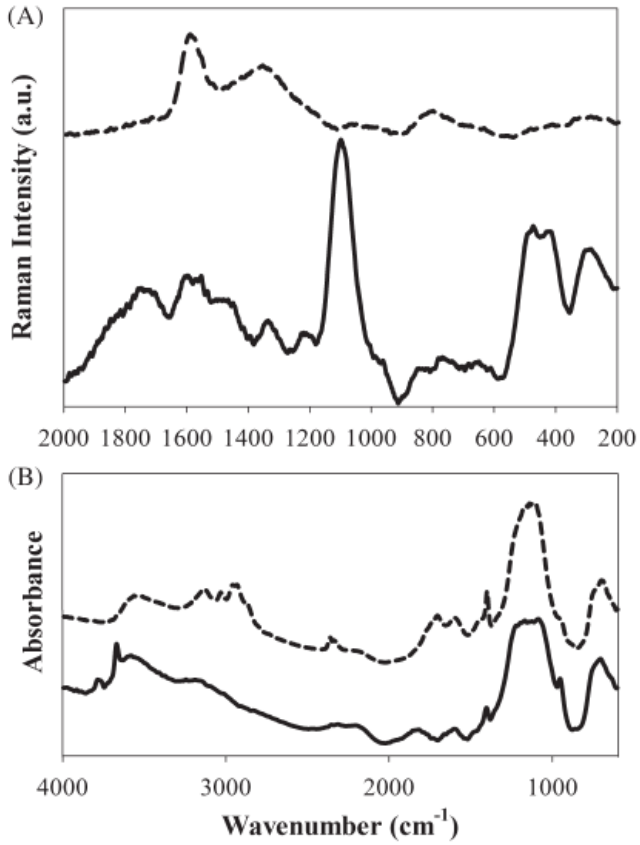


**Figure 11. (**A) Raman spectra and (B)DRIFT spectra of AlPO4450 before ( ‑ ) and after (---) 22 h on stream.

## Conclusions

The presence of a second metal (1 wt% of Co, Cu, Cr, Fe) in the precipitation medium of AlPO4 did not affect its amorphous character and mesoporosity even after being calcined at 450∘C and 650∘C. The modified aluminium phosphates calcined at 650∘C, exhibiting a superficial enrichment of metal, showed the highest activity (near 100%) in the glycerol transformation, regardless of the metal added, with a yield to acrolein oscillating between 49% (AlCuPO650) and 54% (AlCoPO650) at 3 h of time on stream, with 50 mg of catalyst and 280∘C reaction temperature. The yield to the second main product, hydroxyacetone, oscillated between 28% (AlCrPO650) and 33% (AlCuPO650). Furthermore, a change in the formation of dehydration products with time on stream took place on all the phosphates. Thus, the yield to acrolein decreased and similarly the yield to hydroxyacetone increased, attaining values greater than 60% on phosphates modified with Fe and Co, at 22 h. This result could be explained by a change in the equilibrium between Lewis and Bronsted acid sites, favouring the formation of Bronsted sites, given the presence of water in the feed (36 wt% glycerol aqueous solution). None of the phosphates suffered deactivation after 22 h of operation, whereas the zeolites underwent a strong loss of activity, caused by blockage of the micropores, which were predominant, by coke. The formation of coke at the beginning of the reaction, involving strong acid sites, preferably Bronsted acid, has also been verified. Unsaturated and aromatic compounds were the main components of coke.

We propose that on the phosphates studied, the acrolein formation from glycerol could take place preferably through an E2 mechanism involving a pair of Lewis acid and base sites, whereas the hydroxyacetone formation could occur mainly through an E1 mechanism with participation of the Bronsted acid sites. The participation of the Lewis acid (and base) sites associated with the presence of a transition metal, in addition to those

related to aluminium, would explain the greater activity in the glycerol dehydration exhibited by the modified phosphates with respect to AlPO4, as well as their capacity for the propanone formation from 2-propanol.

**Acknowledgements**

Subsidies granted by the Ministerio de Economia, Industria y Competitividad and FEDER funds (Project CTQ2010-18126, ENE2016-81013-R) and Junta de Andalucia and FEDER funds (P11-TEP-7723) are gratefully acknowledged. S. Lopez-Pedrajas is indebted to the Ministerio de Educacion, Ciencia y Deporte for a FPU fellowship. The authors are thankful to the staff at the Central Service for Research Support (SCAI) of the University of Cordoba for their assistance.

**References**

1. OECD-FAO Agricultural Outlook 2015–2024.

2. Gómez-Jiménez-Aberasturi O and Ochoa-Gómez JR, New approaches to producing polyols from biomass. J Chem Technol Biotechnol: 10.1002/jctb.5149 (2017).

3. Quispe CA, Coronado CJ and Carvalho Jr JA, Glycerol: production, consumption, prices, characterization and new trends in combustion. Renew Sust Energ Rev 27:475–493 (2013).

4. Talebian-Kiakalaieh A, Amin NAS and Hezaveh H, Glycerol for renewable acrolein production by catalytic dehydration. Renew Sust Energy Rev 40:28–59 (2014).

5. Katryniok B, Paul S and Dumeignil F, Recent developments in the field of catalytic dehydration of glycerol to acrolein. ACS Catal 3:1819–1834 (2013).

6. Lopez-Pedrajas S, Estevez R, Navarro R, Luna D and Bautista FM, Catalytic behaviour of mesoporous metal phosphates in the gas-phase glycerol transformation. JMolCatal A - Chem421:92–101 (2016).

7. Estevez R, Lopez-Pedrajas S, Blanco-Bonilla F, Luna D and Bautista FM, Production of acrolein from glycerol in liquid phase on heterogeneous catalysts. Chem Eng J 282:179–186 (2015).

8. Chai S-H, Wang H-P, Liang Y and Xu B-Q, Sustainable production of acrolein: investigation of solid acid–base catalysts for gas-phase dehydration of glycerol. Green Chem 9:1130–1136 (2007).

9. Alhanash A, Kozhevnikova EF and Kozhevnikov IV, Gas-phase dehydration of glycerol to acrolein catalysed by caesium heteropoly salt. Appl Catal A - Gen 378:11–18 (2010).

10. Foo GS, Wei D, Sholl DS and Sievers C, Role of Lewis and brønsted acid sites in the dehydration of glycerol over Niobia. ACS Catal 4:3180–3192 (2014).

11. García-Sancho C, Cecilia J, Moreno-Ruiz A, Mérida-Robles J, Santamaría-González J, Moreno-Tost R et al., Influence of the niobium supported species on the catalytic dehydration of glycerol to acrolein. Appl Catal B - Environ 179:139–149 (2015).

12. Kim YT, Jung K-D and Park ED, Gas-phase dehydration of glycerol over silica–alumina catalysts. Appl Catal B - Environ 107:177–187 (2011).

13. Wang Z, Wang L, Jiang Y, Hunger M and Huang J, Cooperativity of Brønsted and Lewis acid sites on zeolite for glycerol dehydration. ACS Catal 4:1144–1147 (2014).

14. Kinage AK, Upare PP, Kasinathan P, Hwang YK and Chang J-S, Selective conversion of glycerol to acetol over sodium-doped metal oxide catalysts. Catal Commun 11:620–623 (2010).

15. Lauriol-Garbey P, Postole G, Loridant S, Auroux A, Belliere-Baca V, Rey P et al., Acid–base properties of niobium-zirconium mixed oxide catalysts for glycerol dehydration by calorimetric and catalytic investigation. Appl Catal B - Environ 106:94–102 (2011).

16. Tao L-Z, Chai S-H, Zuo Y, Zheng W-T, Liang Y and Xu B-Q, Sustainable production of acrolein: acidic binary metal oxide catalysts for gas-phase dehydration of glycerol. Catal Today 158:310–316 (2010).

17. Suprun W, Lutecki M, Haber T and Papp H, Acidic catalysts for the dehydration of glycerol: activity and deactivation. J Mol Catal A - Chem 309:71–78 (2009).

18. Navarro R, Lopez-Pedrajas S, LunaD,MarinasJMand Bautista FM, Direct hydroxylation of benzene to phenol by nitrous oxide on amorphous aluminium-iron binary phosphates. Appl Catal A - Gen 474:272–279 (2014).

19. Bautista FM, Campelo JM, Garcıa A, Luna D, Marinas JM, Quiros RA et al., Influence of acid–base properties of catalysts in the gas-phase dehydration-

dehydrogenation of cyclohexanol onamorphous AlPO4 and several inorganic solids. *Appl Catal A – Gen* **243**:93‑107 (2003).

20. Bautista FM and Delmon B, 1-Butanol dehydration on AlPO4 and modified AlPO4: catalytic behaviour and deactivation. *Appl Catal A - Gen* **130**:47‑65 (1995).

21. Kar KK, Cloeter MD, Fruchey OS, Harner RS, Matyjaszewski K, Nicolay R *et al.*, Polymerization inhibitor composition and method of inhibiting polymerization of distillablemonomers. US Patent 20110290635 A1 (2011).

22. Blanco-Bonilla F, Lopez-Pedrajas S, Luna D, Marinas J and Bautista F, Vanadium oxides supported on amorphous aluminum phosphate: structural and chemical characterization and catalytic performance in the 2-propanol reaction.*JMolCatal A - Chem***416**:105‑116 (2016).

23. Wijzen F, Koch B, Rocha J, Esculcas A, Liegeois-Duyckaerts M and Rulmont A, Texture and structure of amorphous co-precipitated silica-aluminum phosphate catalyst supports. *J Catal* **177**:96‑104 (1998).

24. Tuel A, Caldarelli S, Meden A, McCusker LB, Baerlocher C, Ristic A *et al.*, NMR characterization and Rietveld refinement of the structure of rehydrated AlPO4-34. *J Phys ChemB* **104**:5697‑5705 (2000).

25. Zhang R, Qin Z, Dong M, Wang G and Wang J, Selective oxidation of cyclohexane in supercritical carbon dioxide over CoAPO-5molecular sieves. *Catal Today* **110**:351‑356 (2005).

26. Xingyi Q, Lili Z, Wenhua X, Tianhao J and Rongguang L, Synthesis of copper-substituted aluminophosphate molecular sieves (CuAPO-11) and their catalytic behavior for phenol hydroxylation. *Appl Catal A - Gen* **276**:89‑94 (2004).

27. Laha S, Kamalakar G and Glaser R, Microwave-assisted synthesis of [Cr]APO-5. *Micropor MesoporMater* **90**:45‑52 (2006).

28. Liu SY, Zhou CJ, Liu Q, Liu GC, Huang CJ and Chao ZS, Synthesis of Mesoporous La-, Cu-, and Cr-Doped aluminophosphates and theircatalytic behavior in the dehydration of glycerol. *ChemSusChem* **1**:575‑578 (2008).

29. Campelo JM, Garcia A, Herencia JF, Luna D, Marinas JM and Romero AA, Conversion of alcohols (*α*-methylated series) on AlPO4 catalysts. *J Catal* **151**:307‑314 (1995).

30. Suprun W, Lutecki M and Papp H, TPD-TG-MS investigations of the catalytic conversion of glycerol overMOx-Al2O3-PO4 catalysts. *Chem Eng Technol* **34**:134‑139 (2011).

31. Suprun W, Lutecki M, Glaser R and Papp H, Catalytic activity of bifunctional transition metal oxide containing phosphated alumina catalysts in the dehydration of glycerol. *J Mol Catal A – Chem* **342–343**:91‑100 (2011).

32. Kim YT, Jung K-D and Park ED, Gas-phase dehydration of glycerol over ZSM-5 catalysts. *Micropor MesoporMater* **131**:28‑36 (2010).

33. Dalil M, Carnevali D, Edake M, Auroux A, Dubois J-L and Patience GS, Gas phase dehydration of glycerol to acrolein: Coke on WO3/TiO2 reduces by-products. *JMolCatal A - Chem***421**:146‑155 (2016).

34. Velasquez M, Santamaria A and Batiot-Dupeyrat C, Selective conversion of glycerol to hydroxyacetone in gas phase over La2CuO4 catalyst. *Appl Catal B - Environ* **160 161**:606‑613 (2014).

35. Sato S, Akiyama M, Takahashi R, Hara T, Inui K and Yokota M, Vapor-phase reaction of polyols over copper catalysts. *Appl Catal A - Gen* **347**:186‑191 (2008).

36. Garcia-Sancho C, Moreno-Tost R, Merida-Robles J, Santamaria- Gonzalez J, Jimenez-Lopez A and Maireles-Torres P, Zirconium doped mesoporous silica catalysts for dehydration of glycerol to high added-value products. *Appl Catal A - Gen* **433–434**:179 187 (2012).

37. Liu Q, Zhang Z, Du Y, Li J and Yang X, Rare earth pyrophosphates: effective catalysts for the production of acrolein from vapor-phase dehydration of glycerol. *Catal Lett* **127**:419‑428 (2009).

38. Lourenco J, Fernandes A, Bertolo R and Ribeiro M, Gas-phase dehydration of glycerol over thermally-stable SAPO-40 catalyst. *RSC Adv* **5**:10667‑10674 (2015).